BL1U

Change in Positron Lifetime of Tensile-Deformed Pure Iron after Stress Release and Room-Temperature Aging

M. Fujinami[1], R. Awaji[1], H. Abe[1], A. Yabuuchi[2], T. Hirade[3], N. Oshima[4] and Y. Taira[5]

[1]*Department of Applied Chemistry and Biotechnology, Chiba University, Chiba 263-8522, Japan*
[2]*Institute for Integrated Radiation and Nuclear Science, Kyoto University, Kumatori 590-0494, Japan*
[3]*Nuclear Science and Engineering Center, Japan Atomic Energy Agency, Tokai 319-1195, Japan*
[4]*National Institute of Advanced Industrial Science and Technology, Tsukuba 305-8568, Japan*
[5]*UVSOR Synchrotron Facility, Institute for Molecular Science, Okazaki 444-8585, Japan*

Understanding the formation of lattice defects in metals not only while applying deformation stress but also after releasing stress and subsequent aging is essential for accurately assessing the durability of structural materials. Positron annihilation lifetime spectroscopy (PALS) is an effective technique for examining vacancy-type defects within crystalline materials [1]. Nevertheless, measuring the positron lifetime in metals while applying deformation stress presents significant challenges when using conventional PALS techniques. As a result, most previous studies have conducted positron lifetime measurements on deformed metals only after the deformation stress has been released. It should be noted that the properties of defects within metals may undergo alterations when the deformation stress is released. This study applied PALS to a pure iron specimen subjected to tensile deformation, using the gamma-ray-induced PALS (GiPALS) technique [2].

A well-annealed pure iron specimen (99.99% purity) was elongated to ~7% nominal strain using a small tensile tester installed at the BL1U beamline (Fig. 1). The thickness and gauge width of the test piece were 3 mm and 6 mm, respectively. Positron lifetime measurements were conducted at three different stages following the deformation: (1) under applied stress after elongation, (2) after releasing the tensile stress, and (3) after 3 days at room temperature following the stress release. The results revealed significant changes in the longer positron lifetime component (associated with defect species) across the three conditions. In addition, the intensity of the defect component (I_2) changed from approximately 45% under stress to 60% immediately after unloading, and then decreased to 28% after 3 days of room-temperature aging (Fig. 2).

These findings suggest that tensile stress release leads to additional defect formation, while subsequent room temperature aging facilitates partial defect recovery. Therefore, it is essential to consider both stress release effects and room-temperature aging when characterizing defect structures in deformed metals. This highlights the importance of in situ characterization in studies of deformed structural materials.

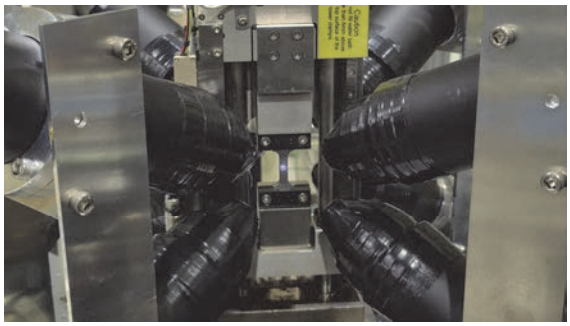

Fig. 1. A view of a small tensile tester installed at the BL1U beamline with a tensile test piece attached.

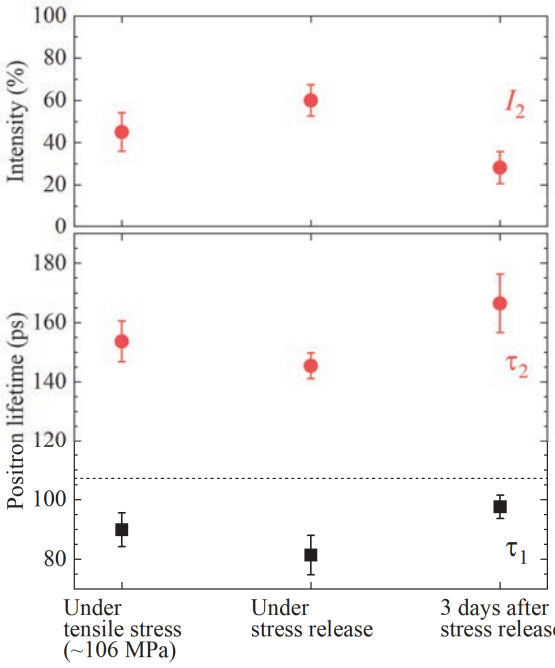

Fig. 2. Positron lifetimes and their intensities of elongated pure iron. The results are shown for the same specimen while applying stress, after releasing the stress, and after aging at room temperature for 3 days. The positron lifetime of the specimen before elongation is also depicted by the dashed line.

[1] R. W. Siegel, Annu. Rev. Mater. Sci. **10** (1980) 393.
[2] Y. Taira *et al.*, Rev. Sci. Instrum. **93** (2022) 113304.

BL1U

Measurements of Temperature-Dependent Absorption Ratios in Transmission Nuclear Resonance Fluorescence

T. Shizuma[1,2], M. Omer[2], R. Hajima[1], M. Koizumi[2], H. Zen[3], H. Ohgaki[3] and Y. Taira[4]

[1]*National Institutes for Quantum Science and Technology, Kizugawa 619-0215, Japan*

[2]*Japan Atomic Energy Agency, Tokai 319-1195, Japan*

[3]*Institute of Advanced energy, Kyoto University, Uji 611-0011, Japan*

[4]*UVSOR Synchrotron Facility, Institute for Molecular Science, Okazaki 444-8585, Japan*

Nuclear Resonance Fluorescence (NRF) is a phenomenon where atomic nuclei absorb and emit γ-rays of specific energies unique to each nuclide. Therefore, by measuring these emitted γ-ray energies, it is possible to identify the nuclide. Additionally, because a γ-ray beam in the MeV energy range is highly penetrating, non-destructive measurement is achievable even when the sample is enclosed in heavy shielding.

In transmission NRF, a γ-ray beam that passes through an absorption target is directed onto another target, called a witness plate (WP), made of the same nuclide as the absorption target. The NRF γ-rays emitted from the WP are then measured. This method is advantageous over scattering NRF as it helps reduce the effects of background radiation [1].

The absorption of γ rays in transmission NRF depends on the temperatures of the absorption and/or WP targets due to variations in the Doppler broadening of the resonant width. As a result, the temperature of the absorption and/or WP targets can affect the measurement's duration and sensitivity. To investigate the temperature dependence of absorption ratios which is defined as $R=1-C/C_0$ where C and C_0 are NRF γ-ray counts with and without the absorption target [2], we irradiated ^{206}Pb samples (both absorption and WP target) at liquid nitrogen (LN_2) temperature using a laser Compton scattering (LCS) γ-ray beam. The LCS γ-rays, with a maximum energy of 5.54 MeV, were produced by the collision of 746-MeV electrons with laser photons of a 1.895 μm wavelength. A 20-cm thick lead collimator with a 3-mm aperture was employed to confine the LCS γ rays, forming the energy width to approximately 8% (FWHM). Two high-purity Ge detectors positioned horizontally at a scattering angle of 90° relative to the incident γ-ray direction were used to measure scattered γ rays from the WP target. The transmitted LCS γ-rays were monitored by a large volume $LaBr_3$ detector placed downstream of the WP target. The experimental setup used for the present measurement is shown in Fig. 1.

Figure 2 shows γ-ray energy spectra measured with (black) and without (red) the absorption target, respectively. Six NRF peaks of ^{206}Pb [3] are observed at 4971, 5037, 5127, 5377, 5470, and 5524 keV. The differences between the intensities at each peak are associated with nuclear resonant absorption (so called self-absorption). The larger the absorption cross section, the greater the difference becomes. The largest self-absorption occurs for the resonance at 5037 keV which has the integrated cross section of 1150 eV b [3]. The measured absorption ratio for this resonance is R=0.68(11) which can be compared with the expected value of 0.58 within the experimental uncertainties. Further analysis is in progress.

This work is in part a contribution of JAEA to IAEA coordinated research program, J02015.

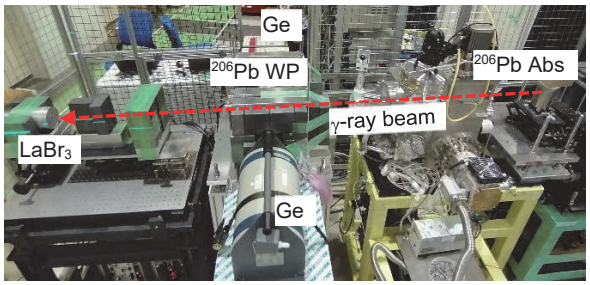

Fig. 1. Photo of the experimental setup used for the present measurement.

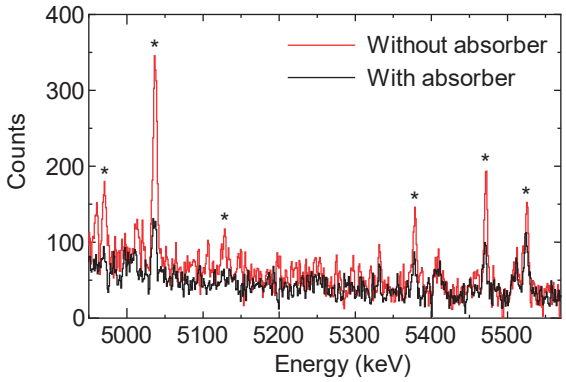

Fig. 2. Energy spectra obtained in transmission NRF experiments. The red (black) spectrum corresponds to the measurement without (with) the absorption target at LN_2 temperature. Asterisks indicate NRF peaks of ^{206}Pb.

[1] C.T. Angell *et al.*, Nucl. Instrum. Methods Phys. Res. B **347** (2006) 11.

[2] F. Metzger, in *Progress in Nuclear Physics*, edited by O. Frisch (Pergamon, New York, 1959), Vol. 7, pp. 53-58.

[3] T. Shizuma *et al.*, Phys. Rev. C **98** (2018) 064317.

Study on 2D Isotope Imaging Using UVSOR-BL1U Undulator

H. Ohgaki[1], K. Nishimoto[1], H. Zen[1], T. Hayakawa[2,3], T. Shizuma[2] and M. Omer[4]

[1]*Institute of Advanced Energy, Kyoto University, Kyoto 611-0011, Japan*

[2]*Kansai Photon Science Institute, National Institutes for Quantum Science and Technology, Kizugawa, Kyoto 619-0215, Japan*

[3]*Institute of Laser Engineering, Osaka University, Suita 565-0871, Japan*

[4]*Integrated Support Center for Nuclear Nonproliferation and Nuclear Security, Japan Atomic Energy Agency, Tokai, Ibaraki 319-1195, Japan*

A flat laser Compton scattering gamma-ray (F-LCS) beam, which has a flat distribution in the energy spectrum and a spatial distribution with a few mm diameter beam size, has been developed to study an isotope selective CT Imaging application at the beamline BL1U in UVSOR[1]. We generate an F-LCS beam by scattering an intense laser beam with a circular-motion electron beam excited by a helical undulator installed at the BL1U beam line. We carried out a proof of principle experiment at the BL1U in UVSOR in 2022 machine time and we obtained a 1D multi-isotope (^{207,208}Pb) imaging using LCS and F-LCS beams in 2023[2].

In 2024, we started evaluation of quantitative information on measured isotopes using an absorption method. We used an absorption target whose composition was one of natural Pb, enriched ^{207}Pb, and ^{208}Pb and three enriched isotope witness targets placed behind the absorption target as shown in Fig.1. The F-LCS beam was generated by using the helical undulator with a K-value of 0.2 as well as normal LCS beam. Most other experimental conditions were the same as the 2023 experiment [2]. To reduce the atomic scattering from the witness targets, the Ge detector angles were changed from 90-deg. in 2023 to 135-deg. We also added the 2nd collimator behind the absorption target to reduce the atomic scattering from the absorption target. The improvement of the background rejection was factor 2 as shown in Fig. 2. Clear NRF peaks from the three witness targets from 5037 keV (^{206}Pb, J^{π}=1$^-$) to 5525 keV (^{206}Pb, J^{π}=1$^-$) were observed. The abundances of ^{207}Pb and ^{208}Pb in the natural Pb target were evaluated by comparison with the NRF yields by the enriched ^{207}Pb and ^{208}Pb targets as the absorption target. The three absorption targets of natural Pb, enriched ^{207}Pb, and ^{208}Pb have the sizes of 5-mm thickness plate, 6.2-mm × 6-mmϕ cylinder, and 15-mm × 8.1-mmϕ (perpendicularly placed). Because the gamma-rays are absorbed by all targets located upstream of the witness target, the thickness correction must be considered for the abundance evaluation. We take into account the atomic absorption in the NRF absorption method, and the result is listed in Table 1[3]. Although the thickness correction to the NRF absorption has not been applied, the evaluated abundances with LCS beams are far beyond the margin of errors. We noticed that the measured $LaBr_3$(Ce) data, which gave the thickness information of the absorption targets, were not reasonable. We are trying to improve the analysis method and figure out the reason for the funny $LaBr_3$(Ce) data.

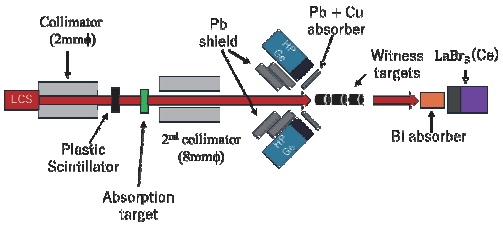

Fig. 1. Schematic drawing of the experiment.

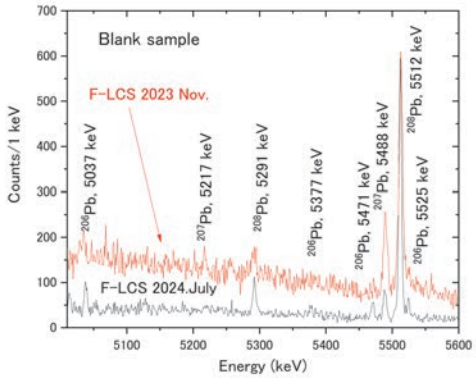

Fig. 2. Measured NRF spectra with the F-LCS beams (red line:2023 Nov., black line: 2024 July).

Table 1. Abundance Evaluation

	Gamma ray beam	^{207}Pb 5488 keV (%)	^{208}Pb 5512 keV (%)
No correction	LCS	−2.9±6.9	46.1±4.2
	F-LCS	11.9±6.2	52.7±5.3
With atomic absorption	LCS	−2.9±6.8	45.7±4.1
	F-LCS	10.6±6.3	52.0±5.3
Established abundance		22.1	52.4

[1] H. Ohgaki *et al.*, Phys. Rev. Accel. Beams **26** (2023) 093402.

[2] H. Ohgaki *et al.*, UVSOR Activity Report **51** (2023) 44.

[3] K. Nishimoto *et al.*, "Quantitative Evaluation of NRF Yield by Using F-LCS beam in UVSOR", AESJ Spring Meeting, online, 2025/03/14.

BL1U

Initial Study of Positron Lifetime Imaging Technique Using Gamma-Ray Beam at UVSOR

S. Takyu[1], Y. Taira[2], T. Hirade[3], F. Nishikido[1], H.G. Kang[1], H. Tashima[1], F. Obata[1], K. Matsumoto[1], M. Takahashi[1] and T. Yamaya[1]

[1]*National Institutes for Quantum Science and Technology (QST), 4-9-1 Anagawa, Inage-ku, Chiba-shi, Chiba 263-8555, Japan*

[2]*National Institutes of Natural Sciences (NINS), 38 NishigoNaka, Myodaiji, Okazaki-shi, Aichi 444-8585, Japan*

[3]*Japan Atomic Energy Agency (JAEA), 2-4 Shirakata, Tokai-mura, Naka-gun, Ibaraki 319-1195, Japan*

Positron emission tomography (PET) is used to diagnose cancer and heart disease, and so on. Unlike CT and MRI, PET can image the internal functions in the living body, and therefore allow us to get closer to the root of internal abnormalities and diseases.

In PET, a positron-emitting drug is administered into the body, and the positrons annihilate with electrons and emit 511 keV photon pairs in the opposite direction, which are detected by a ring-shaped radiation detector. 10^6-10^9 lines of response (LOR) connecting these detection positions are collected, and the drug distribution (radioactivity distribution) is imaged by image reconstruction.

Recently, it has been pointed out that it may be possible to extract new information from the time it takes for positrons to annihilate (lifetime) and use it for diagnosis, because the positron lifetime varies with the surrounding electron density [1]. Therefore, we are currently aiming at the research and development of "quantum PET (Q-PET)" which diagnose by the positron lifetime (Fig. 1.) [2]. To date, we have demonstrated two-dimensional imaging of positron lifetime using a pair of PET detectors [2], and have reported the possibility of imaging hypoxic regions of tumors, which were previously difficult to get quantitative images [3].

However, in living organisms, there are many factors other than oxygen partial pressure that may affect electron density, but there are few basic data that correlates positron lifetime values with diseases. Therefore, the objective of this study is to develop a positron lifetime imaging analysis system that enables three-dimensional analysis of deep inside samples, including living organisms, using 6.6 MeV gamma-ray beam at the UVSOR (Fig. 2. (a)) [4]. Specifically, the beam is irradiated onto the sample, and positrons produced by pair production at the sample depth (to 10 cm) are imaged using the PET principle. The positron lifetime is imaged in three dimensions, with the beam generation as the start and the detection of annihilation photon pairs as the stop. This technique provides accurate information about the start time compared to the technique that accumulates radioisotopes (RIs). This technique also enables three-dimensional analysis of voids in metals and free volume in polymers. This year, we carried out an experiment at UVSOR aimed at the initial demonstration of this technique.

We used one pair of detectors consisting of a 3.2 mm square 8×8 LGSO scintillator array coupled to a 3.2 mm pitch 8×8 MPPC array module. This detector pair was placed opposite each other at a distance of 10 cm, inclined at 15 degrees to the direction of the beam (Fig. 2. (b)). A stainless-steel plate (lifetime value: 106 ps) and a polycarbonate plate (lifetime value: 2.1 ns) were placed separately, and we confirmed the difference in positron lifetime spectra during beam irradiation. We also placed two samples within the field of view of the detector pair and performed simple 2D PET imaging. Details of these achievements will be reported in the conference presentations [5, 6].

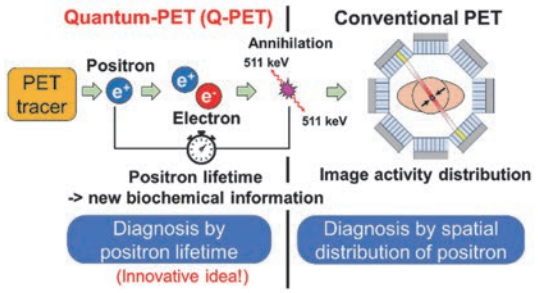

Fig. 1. A difference between quantum PET (Q-PET) and conventional PET.

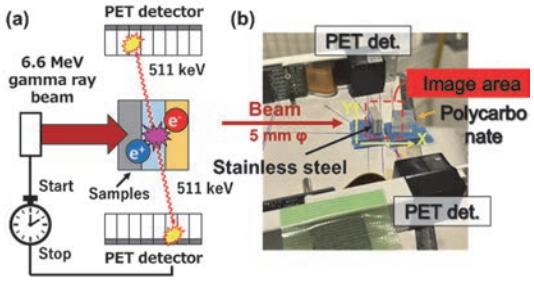

Fig. 2. (a) The principle of the proposed method. (b) The experimental setup.

[1] P. Moskal *et al.,* PET Clin. **15** (2020) 439.
[2] S. Takyu *et al.,* Appl. Phys. Express. **15** (2022) 106001.
[3] S. Takyu *et al.,* Nucl. Instr. Meth. Phys. Res. A. **1065** (2024) 169514.
[4] Y. Taira *et al.,* Rev. Sci. Instrum. **93** (2022) 113304.
[5] S. Takyu *et al.,* Abstract of the 72nd JSAP Spring Meeting 2025, 14p-K502-3, (14, Mach, 2025)
[6] S. Takyu *et al.,* Abstract of the ICPA20, 2025, (submitted)

BL1U

Investigation of Electron Acceleration Location and Condition for Thunderstorm Gamma-ray Flashes

K. Nakazawa[1], A. Tanaka[1], M. Baba[1], Y. Nishimura[1], M. Saito[1], M. Oguchi[1] and K. Okuma[1]
[1]*Graduate school of Sciences, Nagoya University, Nagoya 464-8602, Japan*

Thunderstorm activity is known to produce gamma rays with energies exceeding 30 MeV, which are direct evidence of electron acceleration in the dense atmosphere [1]. Winter thunderstorms along the Sea of Japan is famous for their low-altitude cloud bases (~0.2–0.8 km), which enables ground detection of thunderstorm gamma rays, and we are operating gamma-ray detectors there to understand the location of the acceleration region and its geometry [2-3]. Among them, there are a phenomena called "downward TGFs" which are short duration (< 1 ms), and intense gamma-ray flashes reaching up to 30 MeV [2]. To identify the "origin" of the TGF, we are developing a new detector system, using Cherenkov emission from Compton recoil electron emerged in small acrylic rods, as shown in Fig.1. Our aim is to obtain azimuth and elevation information from the data, and identify the 3D location of the electron acceleration regions, as shown in the right panel of Fig.1.

The detector is made of four acrylic rods, with photo sensors (SiPM) attached to individual ends. As the Cherenkov emission retains some information of the direction of incoming gamma-rays, we can observe the left-right identification of the photon incoming direction by comparing the count rate of the two SiPMs. Although overall performance of the "Cherenkov-rods detectors" have been calibrated using the ~8 MeV gamma-rays from a neutron beam facility KUANS at Kyoto University, the detailed position and angular response of the detector was yet to be understood. We used UVSOR BL1U 6.6 MeV gamma-ray pencil beam and scanned the acrylic rod detector.

We used one acrylic rod for the calibration test in UVSOR. The set up is shown in the left-top panel of Fig.1. Obtained count rates and its ratio as a function of incident angle are summarized in Fig.2. We found that, directed gamma-ray hit to SiPM is non-negligible in side-illumination, while in angled illumination the Cherenkov photon induced events are dominant. The overall angular response is shown in the bottom panel of Fig.2. It reproduced the average profile obtained in the KUANS experiment.

Our experiment in December 2024 was the first time we irradiated a narrow (1 mm) pencil beam to the rod, and found many unexpected, but reasonable phenomena. Based on this result, we are planning more comprehensive experiment to understand the angular response in more detail.

We thank the UVSOR and Dr. Taira for enabling these measurements.

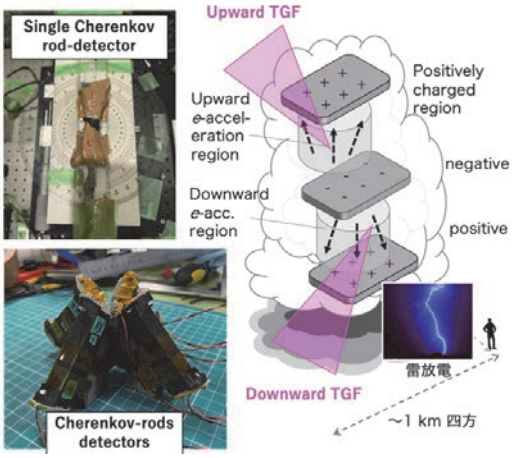

Fig. 1. (right) Concept of our experiment. (left) Our detectors.

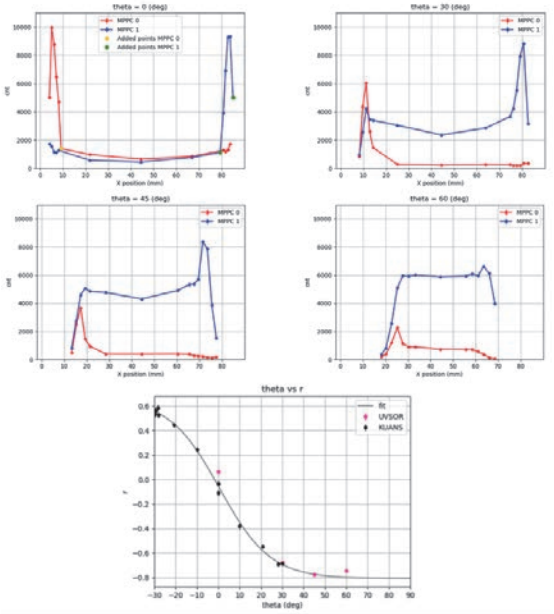

Fig. 2. (top four) Plot of photon count rate vs incident angle. Red is the signals from "right" SiPM and blue is those from "left". (bottom) Angular response as a count-rate ratio as a function of incident angle. UVSOR/BL1U 6.6 MeV result is compared with those obtained in KUANS.

[1] J. R. Dwyer *et al*., Space Sci. Rev. **173** (2012) 133.
[2] T. Enoto *et al*., Nature **551** (2017) 481.
[3] K. Nakazawa *et al*., J. Geophys. Res.:Atmos. **130** (2025) 2024JD042303.

BL1U

Progress in Experimental Study on Single Electron Storage

Y. Asai[1], H. Miyauchi[2, 3], M. Shimada[2, 3] and M. Katoh[2, 4]
[1]*Graduate School of Advanced Science and Engineering, Hiroshima University, Higashi-Hiroshima 739-8526, Japan*
[2]*Research Institute for Synchrotron Radiation Science, Hiroshima University, Higashi-Hiroshima 739-0046, Japan*
[3]*High Energy Accelerator Research Organization (KEK), Tsukuba 305-0801, Japan*
[4]*UVSOR Synchrotron Facility, Institute for Molecular Science, Okazaki 444-8585, Japan*

We have been continuing experimental studies on the single-electron storage at UVSOR-III since 2021 with the aim of conducting fundamental research on the accelerator physics and the electromagnetic radiation from relativistic electrons [1-8]. At BL1U of UVSOR-III, we extracted undulator light in the UV region at a wavelength of 355 nm into the atmosphere through a sapphire window and observed its intensity using a photomultiplier tube with an appropriate band-pass filter to reduce background light. After injecting a small amount of electrons which corresponds to 0.1 mA, the beam current is reduced by using the beam scraper. When the number of the electrons comes to be smaller than a few tens, we observe a step-function-like intensity change with a good SN ratio, that allows us to confirm the number of the stored electrons. When the number of the electrons comes to be unity, we pull out the beam scraper, then the last electron is stored in the ring for longer than several hours.

After establishing the operation technique for the single electron storage described above, we have conducted several experiments, which have been reported elsewhere [3-8]. In this report, we shortly describe a few results from the recent progresses.

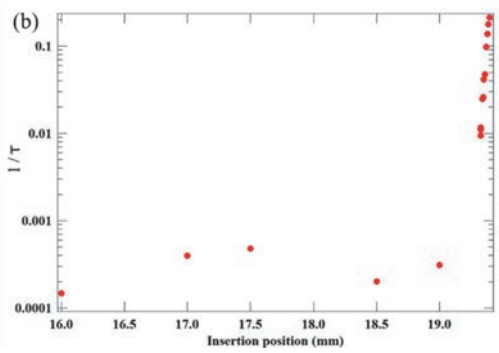

Fig. 1. Beam loss rate vs. Scraper position.

To achieve the single electron storage, we have been using the beam scraper, which is a copper rod installed on the beam pipe. It is inserted to the beam pipe to limit the transverse aperture in the vertical direction. Figure 1 shows the relationship between the insertion position, which is the distance from the pipe wall to the head of the rod, and the beam loss rate. The beam loss rate shows steep increase toward the scraper position around 19.5 mm. The vertical aperture of the beam pipe is 38 mm, which means that the position 19 mm corresponds to the beam center. From the data, the beam center seems to exist at around 19.5 mm. This small discrepancy may arise from the misalignment between the beam and the pipe and also from the mechanical error of the scraper position. When the scraper position is smaller than 19 mm, the beam loss does not show strong dependence on the scraper position. This suggests that, in this range, the beam loss is dominantly caused by the gas scattering or Touschek effect. On the other hand, the beam loss beyond 19 mm is considered to be due to so-called quantum lifetime. Quantitative analysis will be made in near future.

To investigate the properties of radiation from a single electron, we are planning to construct measurement system based on optical fibers, which is expected to make the measurement system more flexible, robust and hard against the background light. We have tested a fiber coupler and a new photomultiplier tube, which is capable of directly producing a photon counting signal without amplifier nor signal processor. The new detector system gave an excellent result in the photon counting measurement.

[1] R. Shinomiya *et al*., UVSOR Activity Report 2021, **40** (2022) 40.
[2] R. Shinomiya *et al*., presented at JSR2022, 9PS01S (Jan., 2022).
[3] Y. Asai *et al*., presented at JSR2023, 1F03S (Jan., 2023).
[4] Y. Asai *et al*., UVSOR Activity Report 2022, **42** (2023) 42.
[5] Y. Asai *et al*., presented at PASJ2023, WEP26 (Aug. 2023).
[6] Y. Asai *et al*., presented at 2023 Annual meeting of JPS, 19aRD11, 3 (Sep., 2023).
[7] Y. Asai *et al*., presented at 2023 HiSOR Symp., P02S (Mar., 2023).
[8] Y. Asai *et al*., presented at 2024 Annual meeting of JPS, 18pB111-11 (Sep., 2024).

BL1U

Spatial Polarization Distribution Measurements of Gamma Rays Produced by Inverse Compton Scattering

Y. Yang[1,3,4], Y. Taira[1,2], T. Shizuma[5] and M. Omer[6]
[1]*Institute for Molecular Science, National Institutes of Natural Sciences, Okazaki 444-8585, Japan*
[2]*School of Physical Sciences, The Graduate University for Advanced Studies (SOKENDAI), Okazaki 444-8585, Japan*
[3]*School of Physics, Zhengzhou university, Zhengzhou 450001, China*
[4]*Shanghai Institute of Applied Physics, Chinese Academy of Sciences, Shanghai 201800, China*
[5]*National Institutes for Quantum Science and Technology, Kizugawa 619-0215, Japan*
[6]*Integrated Support Center for Nuclear Nonproliferation and Nuclear Security, Japan Atomic Energy Agency, Tokai 319-1195, Japan*
Email:yangyuxuan@ims.ac.jp

Polarization measurements of MeV gamma-rays are essential in astrophysics and nuclear physics, offering profound insights into fundamental physical processes [1]. Highly polarized MeV gamma rays can be generated in the laboratory by inverse Compton scattering (ICS) of a polarized laser with a relativistic electron beam. ICS gamma rays possess characteristics such as energy tunable, quasi-monochromatic, and a low divergence angle (<1 mrad). At the UVSOR synchrotron facility, 6.6 MeV gamma rays can be generated by a 90° collisional ICS between a 750 MeV electron beam and an 800 nm laser. The gamma rays are used for user applications such as positron annihilation spectroscopy and detector evaluation of polarized gamma-ray detectors.

By shifting the position of the lead collimator, which is placed on the gamma-ray beam axis, the gamma-ray energy can be changed in the range of 3 ~ 6.6 MeV [2]. However, since the polarization of ICS gamma rays also varies with the position of the beam cross-section, it is necessary to measure the two-dimensional polarization distribution of the gamma rays. We have developed a new polarimeter that can measure the linear polarization of gamma rays in the MeV region. The measurement setup is shown in Fig. 1. The system enables asymmetry analysis of Compton scattering cross-sections using a 50-mm-thick iron target and seven NaI detectors arranged at the scattering angle of 45° with the azimuthal angles spanning 0°~180° in 30° increments. Figure 2 shows the azimuthal distribution of Compton scattered gamma rays when vertically polarized gamma rays are measured, allowing us to measure the asymmetry due to polarization.

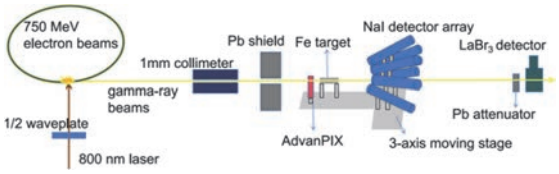

Fig. 1. The Schematic illustration of the spatial polarization distribution measurement.

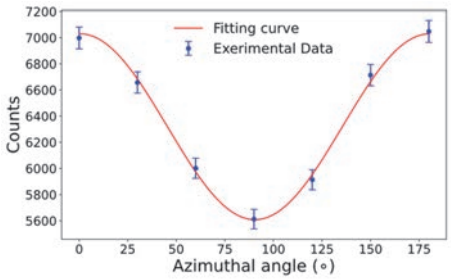

Fig. 2. Azimuthal scattering distribution of vertically polarized gamma-rays when collimator position is horizontal $x = 0$ mm and vertical $y = 4$ mm.

The ICS gamma-ray beam was collimated by a 1-mm lead collimator and then irradiated to the iron target. Two dimensional spatial polarization distribution of ICS gamma rays can be obtained by measuring the azimuthal distribution of Compton scattered gamma rays while shifiting the collimator, target, and detectors in two dimensions. Simultaneously, the gamma-ray beam profile injecting into the target was monitored using an AdvanPIX CdTe image sensor, and the ICS gamma energy spectrum was recorded by a $LaBr_3$ detector. The range of the two dimensional scan was $0 \leq \gamma\theta \leq 1$ and $0 \leq \phi \leq 2\pi$, which sufficiently covers the cross section of the ICS gamma-ray beam, where γ is the Lorentz factor of the electron beam, θ is the scattering angle of gamma rays, and ϕ is the azimuthal angle.

We measured the two-dimensional spatial polarization distribution of horizontally and vertically linearly polarized gamma rays. Building on this methodology, the two-dimensional polarization distributions of ICS gamma rays generated by using a radially and azimuthally polarized laser [3] will be evaluated.

[1] J. Speth *et.al.*, Rep. Prog. Phys. **44** (1981) 719.
[2] Y. Taira *et.al.*, Phys. Rev. A **107** (2023) 063503.
[3] Y. Taira, Phys. Rev. A **110** (2024) 043525.

BL1U

Gamma-Ray Induced Positron Annihilation Lifetime Spectroscopy of Undoped and Bi-Doped $SrTiO_3$ Ceramics

K. Kamoshida[1], M. Kitaura[1], M. Hagiwara[2], H. Masai[3], S. Watanabe[4] and Y. Taira[5,6]

[1]*Facalty of Science, Yamagata University, Yamagata 990-8560, Japan*
[2]*Department of Applied Chemistry, Keio University, Yokohama 223-8522, Japan*
[3]*Department of Materials and Chemistry, National Institute of Advanced Industrial Science and Technology (AIST), Ikeda 563-8577, Japan*
[4]*Innovative Technology Laboratories, AGC Inc., Yokohama 230-0045, Japan*
[5]*UVSOR Synchrotron Facility, Institute for Molecular Science, National Institutes of Natural Science, Okazaki 444-8585, Japan*
[6]*School of Physical Science, The Graduate University for Advanced Studies (SOKENDAI), Okazaki 444-8585, Japan*

Relaxors are dielectrics with substantial energy storage capacity. It is expected that these materials will contribute to the miniaturization and efficiency of diverse electrical systems. However, well-known lead-free ceramics exhibit challenges, including the generation of heat during voltage application, which can markedly reduce the capacitor's lifespan. To address this challenge, the focus has shifted to relaxor dielectrics such as $(Sr,Bi)TiO_3$ (SBT), which are obtained by Bi doping into $SrTiO_3$ (STO). This material has garnered significant attention due to its potential as a solution to the aforementioned issues [1]. The valence of the Bi atom occupying the A site (Sr site) is not equivalent to that of the Sr atom, suggesting the introduction of atomic vacancies to compensate for the charge of the Bi atom at the A site. In this study, we employed gamma-ray induced positron annihilation lifetime spectroscopy (GiPALS) and first-principles calculations based on density functional theory (DFT) to investigate whether atomic vacancies are introduced by Bi doping in STO.

Samples of STO and SBT were ceramics synthesized by the solid state reaction. The experimental details of the GiPALS analysis have been previously reported [2]. To identify the origin of atomic vacancies in SBT, positron annihilation lifetimes were determined by DFT calculation using the ABINIT code [3]. The GiPALS spectra of STO and SBT ceramics are shown in Fig. 1. The data were measured at room temperature. The GiPALS spectra of STO and SBT are characterized by a predominant exponential decay component. The positron annihilation lifetimes of STO and SBT were determined to be 187 ± 1 ps and 291 ± 1 ps, respectively. It is evident that the lifetime of the ceramics undergoes a substantial alteration upon the introduction of Bi doping. This substantial alteration in the lifetime of the ceramics suggests the introduction of atomic vacancies as a consequence of the Bi doping process. The calculated positron annihilation lifetime for the unit cell of STO (bulk lifetime) was 157 ps. The calculated bulk lifetime for STO was nearly equivalent to the experimental bulk lifetime of the STO single crystal (146 ± 2 ps). This outcome serves to substantiate the validity of the experimental approach employed in this study. Furthermore, the calculated lifetimes for the 2×2×2 supercells of STO containing cation vacancies at the A and Ti (B) sites were 277 ps (q=−2) and 195 ps (q=−4), respectively. It is noteworthy that these values exhibited slight variations depending on the valence of the supercell (q). In the STO ceramics, positrons can annihilate at either of dislocations or Ti vacancies at the B sites. The experimental lifetime for the SBT ceramics exhibited agreement with the calculated lifetime for the 2×2×2 supercells of STO containing a Sr vacancy at the A site. In the SBT ceramics, positrons most likely annihilate at Sr vacancies at the A sites. The analysis of the effect of Na and K codoping on vacancies at the A site is currently underway. This work was supported in part by JSPS Grants-in-Aid for Transformative Research Areas (A) Hyper-Ordered Structures Sciences (Nos. 23H04094, 23H04119, 20H05882).

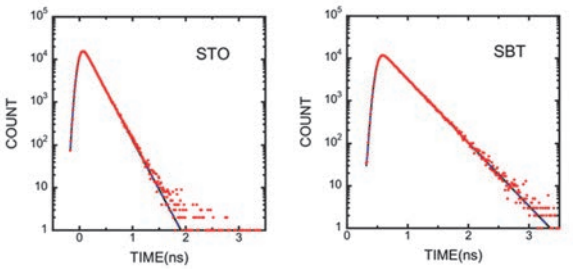

Fig. 1. GiPALS spectra of STO and SBT ceramics, measured at room temperature.

[1] D. Yuqin *et al*., Composites B **230** (2022) 109493.
[2] M. Kitaura *et al*., Opt. Mater.: X **14** (2022) 100156.
[3] X. Gonze *et al*., Comput. Phys. Commun. **248** (2020) 107042.

BL1U

Changes in Positron Annihilation Lifetimes for CeO_2 by Heat Treatment and Re-Adsorption of Oxygen

S. Dohshi[1], K. Maeda[1], Y. Taira[2] and T. Hirade[3]
[1]*Osaka Research Institute of Industrial Science and Technology*
2-7-1, Ayumino, Izumi, Osaka 594-1157, Japan
[2]*UVSOR Synchrotron Facility, Institute for Molecular Science, Okazaki 444-8585, Japan*
[3]*Japan Atomic Energy Agency, Ibaraki 319-1195, Japan*

In the previous study, the authors arranged a cerium oxide (CeO_2) catalyst within a quartz tube and performed gamma-ray induced positron annihilation lifetime spectroscopy (GiPALS) measurements at room temperature in air. The positron annihilation lifetimes of CeO_2 arranged within a quartz tube were nearly equivalent to those of CeO_2 measured without quartz tube. This result suggests that the positron annihilation lifetime measurements of CeO_2 can be performed, even though using quartz tube. Then, the GiPALS measurements were performed on CeO_2 that was arranged within a quartz tube and subjected to treat at 200 °C under argon (Ar) flow, resulting in changing the lifetime component attributed to the annihilation at CeO_2 surface. Additionally, the positron annihilation lifetime spectrum was observed to return to its original state when air containing water vapor was introduced, possibly due to the re-adsorption of oxygen and/or water molecules on the surface defect sites [1]. However, it was uncleared that which gas was re-adsorbed on the surface defect sites.

This study observed the changes in the positron annihilation lifetime spectra as the heating temperature was varied. Additionally, the changes in positron annihilation lifetime spectra were observed when only oxygen was re-adsorbed on CeO_2 treated at 200 °C under Ar flow.

The pellet sample with 20 mm in diameter and 10 mm in thickness were prepared using CeO_2 nanoparticles with a primary particle size of ca. 2 nm. In this experiment, the pellets were heated in a quartz tube at a rate of 10 °C/min using a jacket heater under Ar (purity: 99.999%) flow at pre-determined temperature (50 °C ~ 200 °C) and held for 2 h. After cooling under Ar flow, GiPALS measurements were performed. Finally, oxygen (purity: 99.999%) was flowed through at a rate of 200 mL/min for 1 h at room temperature, followed by another GiPALS measurement under oxygen flow.

We have set up a gamma-ray spectroscopy system at the laser-Compton scattering (LCS) beamline of BL1U at UVSOR-III [2], and measured the lifetime of the annihilation gamma-rays at room temperature using BaF_2 scintillation detector. We used the software Lifetime9 (LT9) to analyze the spectra.

The spectra were changed with the increase in the heating temperature. This is because the positron lifetime increases when heated under Ar flow. Adsorbed active oxygen species have been reported to desorb at temperatures above 150 °C. Consequently, the spectral change below 150 °C can be attributable to desorption of water molecules adsorbed on surface defect sites.

Figure 1 shows the positron annihilation lifetime spectra of CeO_2 at room temperature in air, treated at 200°C under Ar flow, and re-adsorbed oxygen. The positron annihilation lifetime becomes longer when CeO_2 was treated at 200 °C. This change was believed to result from the emergence of oxygen defects on the surface caused by the desorption of adsorption species such as active oxygen and water molecule, as above mentioned. Additionally, the positron annihilation lifetime spectrum was observed not to return to its original state when only oxygen was introduced. Considering the recovery of the spectrum to its original state upon the introduction of air containing water vapor, it can be assumed that there are multiple types of defect sites on CeO_2 surface. Details will be discussed in the future.

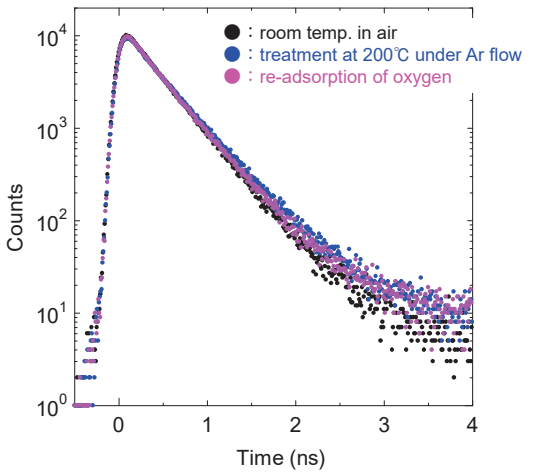

Fig. 1. Positron annihilation lifetime spectra of CeO_2 measured under different conditions.
(a) at room temperature in air, (b) after heating at 200 °C for 2h in Ar, (c) re-adsorption of oxygen.

[1] S. Dohshi *et al*., UVSOR Activity Report **51** (2023) 63.
[2] Y. Taira *et al*., Rev. Sci. Instrum. **84** (2013) 053305.

BL1U

Characterization of Defects in Ni Alloys Based on Gamma-ray-induced Positron Annihilation Spectroscopy

Z. Weixin[1,3], Y. Yuxuan[2,3], Y. Yigang[1] and Y. Taira[3]

[1]*Key Laboratory of Particle and Radiation Imaging (Ministry of Education) and Department of Engineering Physics, Tsinghua University, Beijing 100084, China*

[2]*School of Physics, Zhengzhou University, Science Avenue 100, Zhengzhou 450001, China*

[3]*UVSOR Synchrotron Facility, Institute for Molecular Science, Okazaki 444-8585, Japan*

Positron annihilation spectroscopy (PAS) serves as a powerful non-destructive probe for characterizing atomic-scale defects including vacancy and dislocation in bulk materials. In recent years, gamma-ray-induced positron annihilation spectroscopy (GiPAS) which can be used to study defects in crystals, metals, alloys, and polymers for thick samples (~cm) has developed rapidly [1]. This technology can be used to predict the fatigue and failure of the engineering materials by detecting the volumetric assay of defects at early stage.

The determination of the fatigue and failure level at the early stage before appearing obvious cracks of thick engineering materials is important to evaluate its service life. Inconel 718, a Ni-Fe-Cr austenite (γ) has attracted attention as its particular applications in a variety of applications like gas turbine blades, combustors. We systematically investigate defect evolution in industrial-grade Inconel 718 nickel-based superalloy subjected to incremental tensile deformation (0%, 0.2%, 1%, 2%, 5%, and 10%). GiPAS has been developed at UVSOR [2] and can be used to probe the detects of thick materials. The setup of positron annihilation lifetime spectroscopy (PALS) measurement is shown in Fig1.

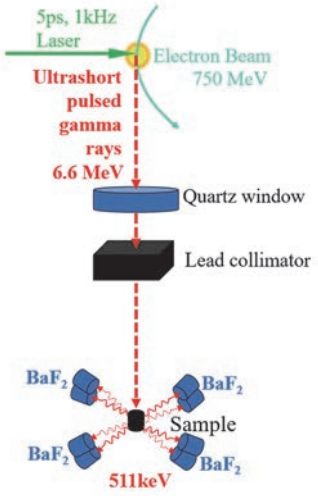

Fig. 1. Setup for PALS measurements.

We implemented PALS coupled with first-principles calculations based on density functional theory (DFT) to quantify defect characteristics. The experimental positron annihilation lifetimes (τ_1 and τ_2) and relative intensities (I_1 and I_2; $I_1+ I_2=1$) are analyzed using LT9 software. The results are shown in Fig2.

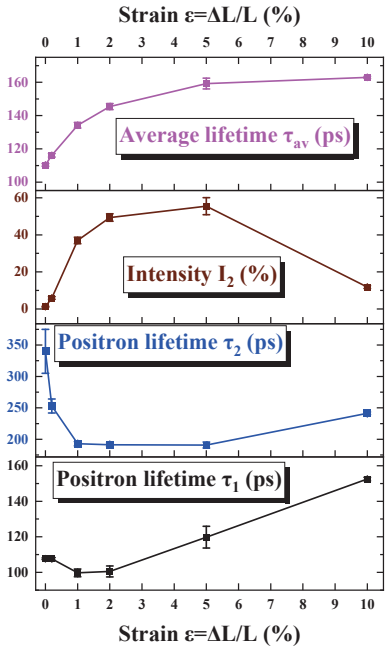

Fig. 2. Fitting results of the experimental positron lifetime spectra.

The calculated free-state positron lifetime of Ni alloy ($Ni_{19}Fe_6Cr_6Nb$) is approximately 106ps. As the positron lifetime τ_1 is larger than this value, it can be considered as a weighted sum of the free-state positron lifetime and the positron lifetime at the dislocation defects. The positron lifetime τ_2 has a range of 190-400ps, which corresponds to the positron lifetime at the vacancy-type defects according to the calculated results. The average positron lifetime tend to increase with increasing tensile strain and indicates that the densities of dislocation and vacancy defects in the sample increase with increasing tensile strain. When the tensile strain reached to 10%, the intensity I_2 has an obvious change which may mean that the defect structure in the sample has changed significantly.

[1] F. A. Selim *et al*., Nucl. Instr. Meth. Phys. A **495** (2002) 154.
[2] Y. Taira *et al*., Rev. Sci. Instrum. **84** (2013) 053305.

BL1U

Photoionized Plasma Production Experiments in the Synchrotron Light Source UVSOR

M Kobayashi[1], S Yoshimura[1], H Ota[2,3], H Chimura[1], K Shimizu[3], T Kaneyasu[3,4] and M Katoh[3,5]

[1]*National Institute for Fusion Science, Toki city 509-5292, Japan*

[2]*Japan Synchrotron Radiation Research Institute, 1-1-1, Kouto, Sayo-cho, Sayo-gun, Hyogo 679-5198, Japan,*

[3]*UVSOR Synchrotron Facility, Institute for Molecular Science, Okazaki city 444-8585, Japan*

[4]*SAGA Light Source, Tosu city 841-0005, Japan*

[5]*Reserach Institute for Synchrotron Radiation Science, Hiroshima University, Higashi-Hiroshima 739-0046, Japan*

Photoexcitation and photoionization are important processes in space to produce plasmas. The photoinduced processes will also become important in divertor region of nuclear fusion reactors due to both the increase in gas pressure and in the emission from plasmas. In the photoionized plasmas, there is no threshold energy to initiate discharge such as Paschen's law in the electric field application. The cross section of the photoionization decays rapidly with increasing photon energy. The photon energy exceeding the ionization potential is converted to kinetic energy of electrons. Owing to these features, photoionized plasmas are expected to have distinct characteristics from those produced by electric field application, which is usual scheme to produce plasmas in laboratory experiments. In particular, the photoionization rate coefficients become large at several tens eV range for most of atoms and molecules. However, photoionized plasma experiments with systematic scan of photon energy in this range have not been performed so far. Therefore, understanding plasma properties, particularly in terms of plasma as collective phenomena of charged particles, is still very limited. In these contexts, we are developing experimental apparatus that can generate photoionized plasmas by using the synchrotron light source [1], which is capable to change the energy of the beam continuously in a wide range, from X-ray, EUV, VUV, visible, to infra-red ranges.

The VUV/EUV beam was produced in the undulator beam line BL1U in UVSOR. The higher-order light of the undulator beam is cut by gold and an aluminum mirror located on the upstream gas cell, as shown in Fig.1. The cut-off energy is selectable by changing an incident angle of the beam to the mirrors, and it was set to 40eV in the present experiments. The gas cell is connected to the beamline with a multi-step differential exhaust system without a vacuum shielding with a window or film, to avoid flux attenuation caused by the window or film. The photon flux of an order of 10^{15} photons/sec/mm^2 with a beam radius of about 1 mm is obtained at the center of the gas cell. Sample gas was introduced to the gas cell in a range from 1 to 10 Pa, while keeping the high vacuum condition, an order of $10^{-6} \sim 10^{-7}$ Pa, at the upstream chamber connected to the storage ring.

The beam energy was scanned from 16 to 36 eV. The production of photoionized plasmas was detected with emission spectra of the gas and the Langmuir probe measurements. Figure 2 shows a camera image of the Ar plasmas produced by beam energy of 22 eV, where the emission along the beam is clearly observed. The estimated plasma parameters are electron density of order of 10^{13} m^{-3} and electron temperature of about 1 eV at a position 1 mm away from the beam axis. The density decays quickly within 2 mm away from the beam, while temperature is almost constant in space. Analysis of emission spectra to evaluate plasma parameters will be conducted for comparison with the Langmuir probe measurements.

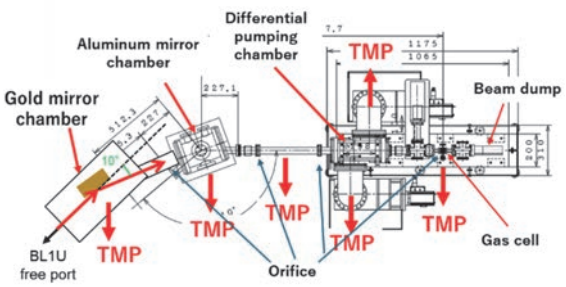

Fig. 1. Schematic of experimental set of photoionized plasma experiments. TMP denotes turbo molecular pump.

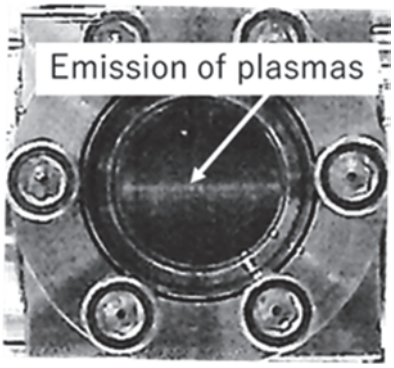

Fig. 2. Visible camera image of photoionized plasmas produced with argon gas of 10 Pa and beam energy of 22 eV. Emission along the beam is clearly observed.

[1] M. Kobayashi *et al.*, Plasma Fusion Res. **19** (2024) 1301038.

BL1U

State-Resolved Molecular Chirality Based on the High-Precision Measurements of Photoelectron Circular Dichroism

H. Kohguchi[1], Y. Hikosaka[2], T Kaneyasu[3], S. Wada[1], K. Shimizu[4], M. Katoh[1,4] and Y-I. Suzuki[5]

[1]*Graduate School of Advanced Science and Engineering, Hiroshima University, Higashi-Hiroshima 739-8526, Japan*

[2]*Institute of Liberal Arts and Sciences, University of Toyama, Toyama 930-0194, Japan*

[3]*SAGA Light Source, Tosu 841-0005, Japan*

[4]*UVSOR Synchrotron Facility, Institute for Molecular Science, Okazaki 444-8585, Japan*

[5]*School of Medical Technology, Health Sciences University of Hokkaido, Tobetsu 061-0293, Japan*

Molecular chirality is generally defined by the molecular structure regarding whether the configuration has a right-handed or left-handed form. Photoelectron circular dichroism (PECD) has been developed as a new approach to examining electronic molecular chirality, which is state-specific and energy-dependent. The BL1U beamline with the undulator is most suited for the PECD study since the circularly polarized light for photoionization is available with the light source in a broad wavelength region. Especially, the BL1U beamline is advantageous for circularly polarized light in the VUV region where PECD is maximized in most chiral molecules [1]. We have investigated the PECD of oxirane with the BL1U beamline and the photoelectron imaging apparatus based on the VMI method.

Oxiranes are typical chiral molecules exhibiting PECD, for which we have conducted the precise measurements of the state- and energy-dependence to compare with our accurate theoretical calculations. The circularly polarized radiation at several wavelengths from 50 nm to 130 nm was used for photoionization. Examples of the observed photoelectron images at various photoionization wavelengths are shown in Fig. 1. The PECD data are difference images between the photoelectron images with the right- and left-circular polarization. The total image intensity was normalized before subtraction. A possible source of inaccuracy occurs in the normalization and background correction of the single polarization image data. The error due to the image data analysis most seriously appears in the highest photoelectron kinetic energy (PKE) region. The photoelectron count rate was suppressed to be lower than 10 kcps by reducing the pulse energy, although the much higher count rate was easily obtained with the BL1U beamline. The number of photoelectrons was limited because our imaging system was too slow to detect correctly more photoelectron spot images on the phosphor screen than 10 kcps. These technical problems could be serious only for the determination of the highly precise PECD parameters. We examined the source of the problems and the solution to improve the accuracy based on the experimental data [2].

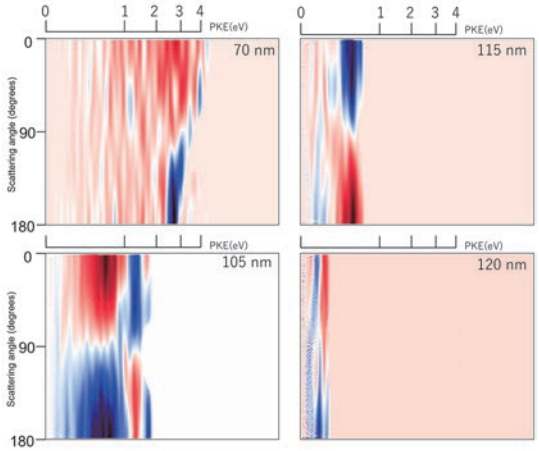

Fig. 1. Photoelectron circular dichroism of methyl oxirane at photoionization wavelengths of 70 nm, 105 nm, 115 nm, and 120 nm. The photoelectron kinetic energy (PKE) is denoted on the upper bar and the scattering angle is indicated on the vertical axis. The partly missing signal region in the largest PKE edge is due to the image data subtraction.

Nevertheless, the state- and energy-dependence of the PECD data are observed (Fig. 1). The PECD was the largest in the low PKE region at the longest photoionization wavelength, which was assigned to the emitted electron from the HOMO and HOMO-1. The sign of PECD (blue/red in Fig. 1) was altered depending on the ionization final states, and the degree of PECD of the particular state varied with the photon energy, therefore PKE. Overall, the PECD decreased with the higher PKE. In the high photon energy (ex. 70 nm in Fig. 1), although the PECD almost disappeared, the highest PKE component exhibited substantially large intensity, indicating a particular state- and energy dependence to reveal the origin of PECD.

[1] H. Kohguchi *et al.*, UVSOR Activity Report **51** (2023) 138.

[2] H. Kohguchi, Y. Hikosaka, T Kaneyasu, S. Wada, and Y-I. Suzuki, UVSOR Activity Report **50** (2022) 136.

BL1U

Inner-Shell Photoelectron Wave Packet Interference by Attosecond Phase Control of XUV Synchrotron Radiation

T. Kaneyasu[1,2], Y. Hikosaka[3], S. Wada[4], H. Ota[5,2], H. Iwayama[2], K. Shimizu[2], M. Fujimoto[6,7] and M. Katoh[8,2,6]

[1]*SAGA Light Source, Tosu 841-0005, Japan*
[2]*Institute for Molecular Science, Okazaki 444-8585, Japan*
[3]*Institute of Liberal Arts and Sciences, University of Toyama, Toyama 930-0194, Japan*
[4]*Graduate School of Advanced Science and Engineering, Hiroshima University, Higashi-Hiroshima 739-8526, Japan*
[5]*Japan Synchrotron Radiation Research Institute, Hyogo 679-5198, Japan*
[6]*Synchrotron Radiation Research Center, Nagoya University, Nagoya 464-8603, Japan*
[7]*Aichi Synchrotron Radiation Center, Seto 480-0965, Japan*
[8]*Research Institute for Synchrotron Radiation Science, Hiroshima University, Higashi-Hiroshima 739-0046, Japan*

The sequential interaction of an atom with a pair of coherent light pulses results in the production of a pair of photoelectron wave packets which interfere with each other during the propagation in a free space. The control and observation of photoelectron wave packet interference has been achieved by using coherent pulse pairs generated by laser sources [1]. Recently, we have shown that the phase coherent double pulses generated by synchrotron light source can be used for controlling the photoelectron wave packet interference in the extreme ultraviolet wavelength [2].

As a next step, we applied this method to the inner-shell ionization of atoms for probing the ultrafast electronic rearrangement processes following the inner-shell ionization of atoms. The experiment was performed by using coherent double pulses generated by a tandem undulator at BL1U. The central photon energy of the pulse was set to approximately 93 eV. The time delay between the pulses was adjusted in femtosecond range with an attosecond resolution. The photoelectron interferogram which comprises of photoelectron spectra measured as a function of time delay, was obtained for helium 1s and xenon 4d photoelectrons.

Figure 1 shows the measured photoelectron interferograms. The interferogram exhibits a periodic modulation due to the interference with a period of approximately 45 as, which corresponds to the photon frequency calculated as $\omega = (E+E_{IP})/\hbar$ where E and E_{IP} are the kinetic energy of the photoelectron and the ionization potential of the atom, respectively. When comparing the two measurements, the contrast of interference quickly decreases as the time delay increases for xenon atoms. This can be explained by the femtosecond Auger decay following the inner-shell ionization. Moreover, the interferogram exhibits intensity modulation with a period of about 2 fs. This effect can be attributed to the evolution of the spin-orbit wave packet produced in the Xe^+ ion, suggesting that this method could be used to explore ultrafast quantum state dynamics with attosecond resolution.

[1] M. Wollenhaupt *et al*., Phys. Rev. Lett. **89** (2002) 173001.
[2] T. Kaneyasu *et al*., Sci. Rep. **13** (2023) 6142.

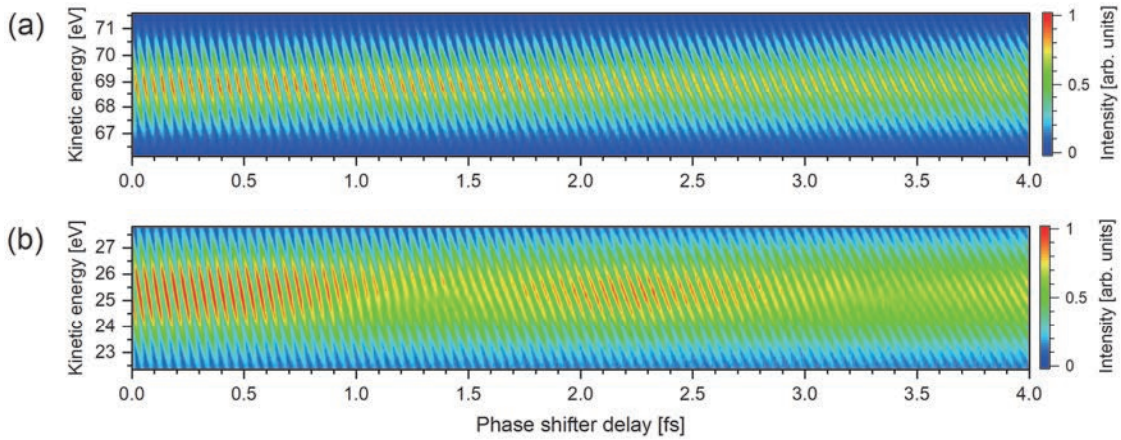

Fig. 1. Photoelectron interferograms measured for (a) helium 1s and for (b) xenon 4d photoelectrons.

BL1U

Circularly Polarized Lyman-α Light Irradiation on Racemic Amino Acid Film to Verify the Cosmic Scenario of Origin of Homochirality

M. Kobayashi[1], K. Matsuo[2], M. I. A. Ibrahim[2], H. Chimura[1], J. Takahashi[3], K. Shimizu[4], H. Ota[4,5], Y. Satake[6], T. Minato[7], N. Takada[7], G. Fujimori[7], K. Kobayashi[8,9], Y. Kebukawa[9], M. Katoh[2,4] and H. Nakamura[1,6]

[1]*National Institute for Fusion Science, Toki city 509-5292, Japan*
[2]*Reserach Institute for Synchrotron Radiation Science, Hiroshima Univ., Higashi-Hiroshima 739-0046, Japan*
[3]*Graduate School of Maritime Sciences, Kobe University, Kobe 658-0022, Japan*
[4]*UVSOR Synchrotron Facility, Institute for Molecular Science, Okazaki city 444-8585, Japan*
[5]*Japan Synchrotron Radiation Research Institute, 1-1-1, Kouto, Sayo-cho, Sayo-gun, Hyogo 679-5198, Japan*
[6]*Nagoya University, Furo-cho, Chikusa-ku, Nagoya 464-8601, Japan*
[7]*Institute for Molecular Science, Okazaki city 444-8585, Japan*
[8]*Department of Chemistry and Life Science, Yokohama National University, Yokohama 240-8501, Japan*
[9]*Department of Earth and Planetary Sciences, Institute of Science Tokyo, Meguro-ku, Tokyo 152-8550 Japan*

The homochirality of life remains one of the most enigmatic issues in the study of the origin of life. A proposed mechanism for symmetry breaking involves irradiation by circularly polarized light (CPL). To investigate the photoreaction of amino acids induced by vacuum ultra-violet (VUV) CPL irradiation, we performed experiments where amino acids in a solid state were irradiated with CPL. This study focuses on Lyman-α (121.6 nm in wavelength), a leading candidate for selective photolysis when circularly polarized.

To investigate the photoreaction of amino acids caused by VUV CPL irradiation, we developed a VUV CPL irradiation system at the beamline BL1U in UVSOR at the Institute for Molecular Science [1]. Lyman-α CPL was generated in BL1U, and racemic alanine film specimens were irradiated with this CPL beam. After irradiation, distinct optical activity was observed, with positive and negative values of the optical anisotropy factor for right-handed (R) -CPL and left-handed (L) -CPL irradiation, respectively. However, the anisotropy factor spectra are broad in the measured wavelength range of 180–240 nm, differing from those of enantiopure alanine samples [1]. These results suggest that Lyman-α CPL irradiation not only caused simple preferential photolysis of enantiopure alanine molecules but also introduced additional effects such as oligomerization or polymerization.

These effects were corroborated by LC-MS analysis. The non-irradiated alanine sample predominantly displayed a single peak corresponding to the protonated alanine monomer $[Ala + H]^+$ (NH_3^+-$CHCH_3$-COOH) of m/z = 90. In contrast, the Lyman-α light-exposed samples exhibited additional complex peaks, which suggest the formation of larger molecules, such as oligomeric alanine adducts or modified oligomers, as inferred from their fragmentation patterns with high abundances of m/z values in the range 170 – 450.

It was also observed that Lyman-α CPL irradiation induced the formation of circular network ag-aggregates on the order of 100 nm in the surface of the alanine film with scanning probe microscopy (SPM) measurements, as shown in Fig.1. These results may suggest dimerization, polymerization, or micro-crystallization induced by the high photon energy of the Lyman-α CPL. Further investigations are ongoing to study the photoreaction of amino acids caused by VUV CPL irradiation.

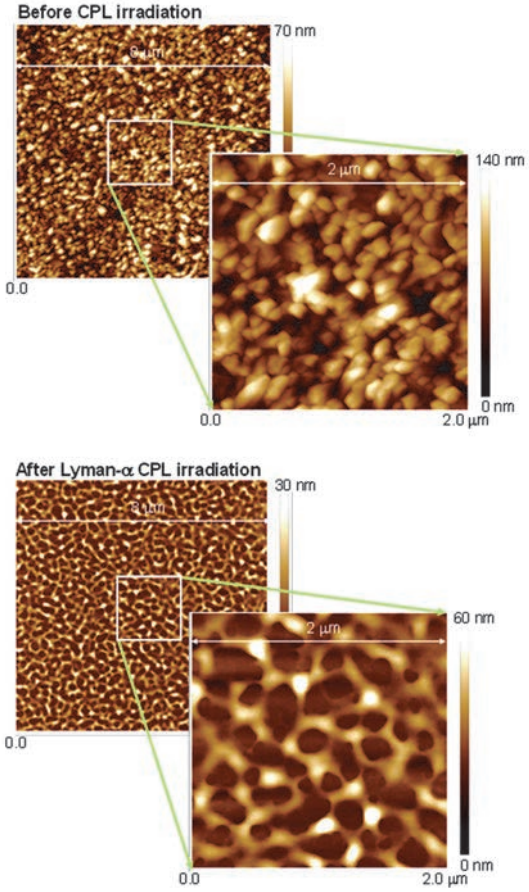

Fig. 1. Topographic images of the DL-alanine film obtained by SPM before (upper) and after (lower) CPL irradiation.

[1] M. Kobayashi *et al.,* Chirality **36** (2024) e70004.

BL1U

Experimental and Theoretical Studies Towards Observing Interactions between Biomolecules and Ultraviolet Optical Vortex

K. Matsuo[1,3,4], H. Kawaguchi[2], R. Imaura[3], S. Hashimoto[3], Y. Nishihara[4], H. Ota[5] and M. Katoh [1,3,4,5]

[1]*Reseach Institute for Synchrotron Radiation Science, Hiroshima University, Higashi-Hiroshima 739-0046, Japan*
[2]*Muroran Institute of Technology, Muroran 050-8585, Japan*
[3]*Graduate School of Advanced Science and Engineering, Hiroshima University, Higashi-Hiroshima 739-8526, Japan*
[4]*School of Science, Hiroshima University, Higashi-Hiroshima 739-8526, Japan*
[5]*UVSOR Synchrotron Facility, Okazaki 444-8585, Japan*

Chirality is an important structural factor in understanding the properties and functions of materials. Circular dichroism spectroscopy using right- and left-handed circularly polarized light with spin angular momentum (SAM: *s*) can observe the chirality of biomolecules in the ultraviolet region below 300 nm. On the other hand, right- and left-handed optical vortex with orbital angular momentum (OAM: *l*) are also expected to be a method for observing chirality, but there are few reports of observations of the interaction between the chirality of biomolecules and optical vortex [1-3], because a method for generating optical vortex in the ultraviolet region has not been established. In this study, in order to observe the interaction between an ultraviolet optical vortex and a biomolecule, we constructed an experimental system which can monitor the ultraviolet absorption of optical vortex using a synchrotron radiation undulator [4-5], and theoretically verified the interaction between an optical vortex and a chiral structure using a finite-difference time-domain method [6].

The second-harmonic light from the helical undulator, which is circularly polarized optical vortex ($s = l = +1$; $s = l = -1$) in the ultraviolet region, is introduced to an optical system consisting of a sample holder, a focusing lens, and a mini-monochromator, which enable the absorption measurement of the circularly polarized optical vortex. To confirm the generation of an optical vortex in the ultraviolet region, a triangular aperture was placed at the sample position, and the optical image was observed with a CCD camera, revealing characteristic scattering patterns indicating right- and left-handed optical vortex [7].

As a chiral sample, the absorption of right- and left-handed optical vortex of + (plus) and – (minus) type *10* camphorsulfonic acid (CSA) was observed at 290 nm. Both the circular dichroism and helical dichroism (Differences in absorbance between right- and left-handed optical vortex) of CSA showed positive and negative values for the + and – types, respectively, but an increase in the intensity of the helical dichroism was observed.

Using the moment method, a type of finite-difference time-domain method, we placed a helical coil at the center of a circularly polarized optical vortex field (or circularly polarized field) (Fig. 1) and theoretically observed the helical dichroism (or circular dichroism) from the scattering intensity of the interaction between the optical vortex (or circularly polarized light) and the coil. With a single coil, the intensity of the helical dichroism was smaller than the circular dichroism, but with two or three parallel coils, the difference between the helical and circular dichroism became smaller. Furthermore, when one coil was moved to the radial direction from the center point of the vortex field, the difference between the helical and circular dichroism became smaller. These theoretical results suggest that the position of a chiral sample relative to the optical vortex field strongly affects their interaction, and indicate the need to take the sample position into account when measuring optical vortex absorption.

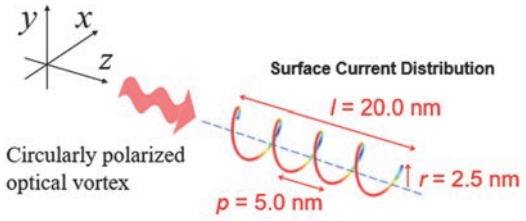

Fig. 1. Helical coil at the center of a circularly polarized optical vortex field for theoretical calculations of helical dichroism (or circular dichroism).

[1] Brullot *et. al.*, Sci. Adv. **2** (2016) e1501349.
[2] Ni *et. al.*, ACS Nano **15** (2021) 2893.
[3] Rouxel *et. al.*, Nat. Photonics **16** (2022) 570.
[4] Katoh *et. el.*, Sci. Rep. **7** 6130 (2017) & Phys. Rev. Lett. **118** (2017) 094801.
[5] Kaneyasu and Katoh *et. al.*, Phys. Rev. A, **95** (2017) 023413.
[6] Kawaguchi, Int. J. Appl. Electromagn. Mech., **65** (2021) 17.
[7] Y. Nishihara *et al.*, UVSOR Activity Report **51** (2024) 47.